## Title
Equilibrium Theory of Bidensity Particle-Laden Flows on an Incline



## ISBN
9783319164588

## Authors
Lee, Sungyon
Wong, Jeffrey
Bertozzi, Andrea L

## Publication Date
2015

## DOI
10.1007/978-3-319-16459-5_4

Peer reviewed

# Chapter 4
# Equilibrium Theory of Bidensity Particle-Laden Flows on an Incline

**Sungyon Lee, Jeffrey Wong and Andrea L. Bertozzi**

**Abstract** The behaviour of inhomogeneous suspensions in a viscous oil is relevant in the context of oil spill and other oil-related disasters which may lead to the unwanted mixture of sand grains and oil. This warrants the fundamental study of the dynamics of solid particles in a thin film of viscous fluid. Specifically, sheared concentrated suspensions in a viscous fluid are subject to a diffusive mechanism called shear-induced migration that consists of "drift diffusion" and "self or tracer diffusion". Drift diffusion causes particles to move from high to low concentrations, while tracer diffusion dictates mixing between particles of the same size. The latter mechanism becomes important in polydisperse slurries. In this chapter, we incorporate the effects of shear-induced migration and sedimentation to develop a model for the gravity-driven thin film of bidensity suspensions. We use this mathematical model to validate recent experimental results.

## 4.1 Introduction

Particle-laden flows are ubiquitous in nature and in industrial applications; however, the nonlinear coupling between particles and fluid motion presents challenges in the development of mathematical models. In the case of monodisperse slurries, there have been advances both in experiments and modelling based on diffusive flux phenomenology [12] and, more recently, suspension balance approach [17]. In particular, [12] developed a diffusive model to justify the behaviour of sheared monodisperse

S. Lee (✉)
Departmant of Mechanical Engineering, Texas A&M,
College Station, TX 77843, USA
e-mail: sungyon.lee@tamu.edu

J. Wong · A.L. Bertozzi
Department of Mathematics and Applied Mathematics Laboratory,
University of California, Los Angeles, CA 90095, USA
e-mail: jtwong@math.ucla.edu

A.L. Bertozzi
e-mail: bertozzi@math.ucla.edu



M. Ehrhardt (ed.), *Mathematical Modelling and Numerical Simulation of Oil Pollution Problems*, The Reacting Atmosphere 2, DOI 10.1007/978-3-319-16459-5_4

suspensions in a Couette device [6]. In the presence of shear, particles undergo a random walk that results in no net displacement. This source of diffusive flux is called "shear-induced self or tracer diffusion" [12, 13]. In the case of non-uniform concentrations in shear, particles tend to drift from regions of high to low particle concentrations due to particle collisions, which is referred to as "drift diffusion" [13]. While effective shear diffusivity consists of both drift diffusion and aforementioned tracer-diffusion, drift diffusion dominates in the case of concentrated monodisperse suspensions.

While both diffusive flux models and suspension balance models have been successful in capturing the particle migration behaviour under shear, they differ substantially in their derivation of particle flux. The diffusive flux phenomenology consists of semi-empirical laws that describe particle migration based on irreversible particle collisions and does not account for the non-Newtonian viscosity of the particle-fluid mixture. The suspension balance approach, on the other hand, relies on the non-Newtonian normal stresses induced by shear, which give rise to the particle migration. Therefore, viscously generated normal stresses are crucial in the suspension balance approach. In particular, the anistropic normal stresses have been shown to be important in predicting correct secondary flows in a pressure-driven tube flow [20]. Thus, the neglect of normal stress differences in the diffusive flux model is problematic especially in the non-dilute concentration limit, as Couturier and co-authors [3] experimentally demonstrated the significance of normal stress differences for the volume fraction greater than 0.17.

Despite the apparent limitations, the diffusive flux approach is "contained" within the suspension balance model and can yield the same set of equations in the unidirectional, fully-developed flows [17]. For instance, Timberlake and Morris [24] experimentally and theoretically studied the gravity-driven, free-surface flow containing neutrally buoyant particles. They observed the deformation of the free surface and particle migration, which sufficiently matched their mathematical model. Although their model was based on the suspension balance approach, the resultant equations for the flux of particles were essentially identical to those derived based on diffusive flux approach of [16]. More recently, [21] observed the accumulation and depletion of the particles on the advancing meniscus and found that, based on the suspension balance model, this depended on the balance between gravitational flux and shear-induced migration. This particular result corresponds exactly to the findings of [15] who identified different particle regimes at varying inclination angles and particle volume fractions based on the diffusive flux approach, further demonstrating the validity of the simpler diffusive flux model in primarily unidirectional flows.

Contrary to the monodisperse case, tracer diffusion becomes important in polydisperse suspensions. Reference [25] investigated the resuspension of heavy particles in a Couette device, with the addition of neutrally buoyant particles of the equal size. At a given shear rate, they found that an increasing concentration of neutrally buoyant particles caused the heavy particles to rise higher to mix with neutrally buoyant ones on the free surface. Based on diffusive flux phenomenology, Tripathi and Acrivos derived a continuum model to match the experimental observations and found that the tendency of particle species to mix is attributed to tracer diffusivity.

In the current work, we extend the equilibrium model of [15] to thin free surface flows of bidensity suspensions. This equilibrium theory is a crucial component of the dynamic problem, since the leading order dynamic equations have shock solutions whose structure is determined by the equilibrium profiles [14, 26]. This warrants a careful study of the equilibrium problem before proceeding to the dynamic case, analogous to the work of [16]. Distinct from the monodisperse case, tracer diffusivity is included in the bidensity model and compared to recent experimental results by [9]. This work provides an important theoretical framework for segregating particles of different densities, which has industrial applications.

This chapter is organized as follows. In Sect. 4.2, we introduce the governing equations for bidensity suspensions and develop the equilibrium model by applying lubrication approximations. In Sect. 4.3, we obtain the solution to the equilibrium model for varying parameters to validate previous experimental results. The chapter concludes with the summary of results and discussion of future directions in Sect. 4.4.

## 4.2 Problem Formulation

We consider the dynamics of a bidensity slurry flowing down an incline, in which the mixture consists of a viscous fluid with density $\rho_l$ and viscosity $\mu_l$ and two species of negatively buoyant particles (See Fig. 4.1). The two particle types have uniform diameter $d$ but variant densities, $\rho_1$ and $\rho_2$, such that $\rho_2 > \rho_1 > \rho_l$. The local volume fractions of each species are denoted as $\phi_1$ and $\phi_2$, respectively, while $\phi = \phi_1 + \phi_2$ is the total volume fraction. By assuming a sufficiently small particle size, the particle-fluid mixture is modelled as a continuum and is governed by the following momentum equations:

$$\rho\left(\partial_t \mathbf{u} + \mathbf{u}\cdot\nabla\mathbf{u}\right) = \nabla\cdot\left(-p\mathbf{I} + \mu(\nabla\mathbf{u} + \nabla\mathbf{u}^\top)\right) + \rho\mathbf{g}, \tag{4.1}$$

where $\mathbf{u}$ and $p$ are the velocity vector and pressure, respectively, and $\mathbf{g}$ denotes the gravitational acceleration vector. As in [15, 16], the mixture density, $\rho$, is given by $\rho = \rho_1\phi_1 + \rho_2\phi_2 + \rho_l(1-\phi)$, while effective viscosity $\mu = \mu_l\,(1-\phi/\phi_\mathrm{m})^{-2}$, where $\phi_\mathrm{m}$ is the maximum volume fraction. In addition to momentum, we have mass conservation of the mixture:

$$\partial_t\rho + \nabla\cdot(\rho\mathbf{u}) = 0. \tag{4.2}$$

The velocity satisfies the no-slip condition ($\mathbf{u} = 0$) on the bottom of the channel, while the stresses vanish both in normal and tangential directions on the free surface: $\mathbf{n}\cdot\left(-p\mathbf{I} + \mu(\nabla\mathbf{u} + \nabla\mathbf{u}^\top)\right) = 0$. The free surface also satisfies the kinematic boundary condition, $\mathbf{n}\cdot\mathbf{u} = 0$.

The conservation equation for particles is given by

$$\partial_t \phi + \mathbf{u} \cdot \nabla \phi + \nabla \cdot \mathbf{J} = 0, \tag{4.3}$$

which accounts for the advection of particles due to flow ($\mathbf{u} \cdot \nabla \phi$) and particle diffusion ($\nabla \cdot \mathbf{J}$), where $\mathbf{J}$ is the particle flux vector that is semi-empirically constructed [13, 19]. For particle-laden flows down an incline, effects of gravity and shear flow govern the particle dynamics inside the thin film, leading to *sedimentation* [4] and *shear-induced migration* [13, 19] of particles that opposes settling. The expressions for $\mathbf{J}$ that account for these competing effects have been derived and experimentally validated for the monodisperse case [2, 15, 16]. For a bidensity slurry in the same geometry, the same physical effects of gravity and shear are present, with added complexities due to the presence of two particle species. By combining previous works [7, 15, 16, 25] and recent experimental results [10], we construct a new particle flux vector $\mathbf{J}$ that accounts for the mixing and sedimentation of two particle species at varying rates.

Based on the formulation by [22, 25], the flux of the $i$th particle species due to sedimentation corresponds to

$$\mathbf{J}_{\mathrm{grav},i} = \frac{\mathbf{g} d^2 \phi_i}{18 \mu_l} \left[ M_0 (\rho_i - \rho_l) + M_I \sum_{j=1}^{2} (\rho_j - \rho_l) \frac{\phi_j}{\phi} \right], \tag{4.4}$$

where $i = 1, 2$. The first term in Eq. (4.4) refers to the self-mobility of particles, $M_0 \sim 1 - \phi/\phi_\mathrm{m}$ [25]. The second contribution to sedimentation comes from interaction mobility, $M_I \sim f(\phi) - M_0$, where the hindrance function $f(\phi) = \mu_l (1 - \phi)/\mu(\phi)$ [13, 15, 16]. The total flux due to sedimentation, $\mathbf{J}_\mathrm{grav}$, is given by $\mathbf{J}_\mathrm{grav} = \mathbf{J}_{\mathrm{grav},1} + \mathbf{J}_{\mathrm{grav},2}$.

As well as settling due to gravity, particles are subject to shear flow inside the thin film and undergo two types of shear-induced diffusion processes [11, 13]. The first type—shear-induced "drift" diffusion—refers to the net drift of particles from the regions of high to low total particle concentration and also from high to low shear stress [12, 19]. In the thin free-surface flows, this diffusive mechanism causes particles to aggregate near the free surface where shear stress vanishes [2, 15, 16]. Since drift diffusion does not distinguish between particle types of equal size, we use the empirical model for particle flux, $\mathbf{J}_\mathrm{drift}$, as used in [2, 15, 16]:

$$\mathbf{J}_\mathrm{drift} = -\frac{d^2 \phi}{4} \left[ K_c \nabla (\dot{\gamma} \phi) - K_v \frac{\phi \dot{\gamma}}{\mu(\phi)} \frac{d\mu}{d\phi} \nabla \phi \right], \tag{4.5}$$

where $K_c$ and $K_v$ are empirically determined constants, and $\dot{\gamma} = \frac{1}{4} \| \nabla \mathbf{u} + \nabla \mathbf{u}^\top \|$ is the shear rate. The corresponding flux for each species is $\mathbf{J}_{\mathrm{drift},i} = \mathbf{J}_\mathrm{drift} \phi_i / \phi$.

The second type of shear-induced diffusion is known as shear-induced "tracer"- (or self-) diffusion [1, 5, 7, 13, 23, 25]. Distinct from drift diffusion, it refers to the

random motion of particles in shear that occurs even in the absence of concentration gradient and leads to zero net drift of particles. While tracer diffusion does not affect $\phi$, it governs how one particle species mixes with the other in bidensity suspensions, resulting in the flux of individual species:

$$\mathbf{J}_{\text{tracer},i} = -\frac{\dot{\gamma} d^2}{4} D_{\text{tr}}(\phi)\phi \nabla \left(\frac{\phi_i}{\phi}\right), \tag{4.6}$$

where $D_{\text{tr}}(\phi)$ is the tracer diffusivity and dictates the extent of mixing in our model. In the limit of dilute suspensions, [11, 13] proposed the empirical expression $D_{\text{tr}} = \phi^2/2$. For large concentrations, numerical simulations and experiments [23] suggest that the tracer diffusivity becomes constant beyond a value $\phi_{\text{tr}} \approx 0.4$. Therefore, we use the expression: $D_{\text{tr}}(\phi) = \frac{1}{2}\min\{\phi^2, \phi_{\text{tr}}^2\}$.

Combining Eqs. (4.4)–(4.6) yields the total flux of the $i$th species, $\mathbf{J}_i$,

$$\mathbf{J}_i = \mathbf{J}_{\text{grav},i} + \frac{\phi_i}{\phi}\mathbf{J}_{\text{drift}} + \mathbf{J}_{\text{tracer},i}, \tag{4.7}$$

and the total flux $\mathbf{J}$ of both species simply corresponds to $\mathbf{J} = \mathbf{J}_{\text{grav}} + \mathbf{J}_{\text{drift}}$. Notably, tracer diffusion drops out of the total particle flux (i.e. $\mathbf{J}_{\text{tracer},1} + \mathbf{J}_{\text{tracer},2} = 0$), justifying its neglect in modelling monodisperse slurries [2, 15, 16, 19]. In addition, Brownian diffusion is not included in particle fluxes by assuming a large Péclet number, or $\text{Pe} = \dot{\gamma} d^2/D \gg 1$, where $D$ is the solvent diffusivity.

### 4.2.1 Thin Film Approximations and Equilibrium Theory

A thin film geometry [18] gives us the following dimensionless variables:

$$(\widehat{x}, \widehat{z}) = \frac{1}{H}(\delta x, z), \quad \widehat{\mathbf{u}} = \frac{1}{U_0}\left(u, \frac{w}{\delta}\right), \quad \widehat{\mathbf{J}} = \frac{H^2}{d^2 U_0}\left(\frac{J_x}{\delta}, J_z\right),$$
$$\widehat{p} = \frac{H}{\mu_l U_0} p, \quad \widehat{\mu} = \frac{\mu}{\mu_l}, \quad \widehat{\rho}_{s,i} = \frac{\rho_i - \rho_l}{\rho_l},$$

where $H$ and $L$ are the characteristic film thickness and axial length scale, respectively, and $U_0 = H^2 g \sin\alpha/\nu_l$. Hats denoting the dimensionless quantities will be subsequently dropped for brevity. In the thin film limit of $\delta \equiv H/L \ll 1$, the momentum equation in the axial direction reduces to

$$\sigma' = -(1 + \rho_{s,1}\phi_1 + \rho_{s,2}\phi_2), \tag{4.8}$$

where $\sigma = \mu(\phi)\partial u/\partial z$ is the dimensionless shear stress, and the prime denotes the derivative with respect to $z$. In addition, we assume $\delta \ll (d/H)^2 \ll 1$, which

reduces Eq. (4.3) to $J_z' = 0$ at leading order. This scaling indicates that particles must rapidly equilibrate in the the $z$-direction [16]. Integrating $J_z' = 0$ with respect to $z$ and applying $J_z(z = 0) = 0$ yields $J_z = 0$, or

$$0 = \phi\sigma' + \sigma\phi'\left[1 + c_1\frac{\phi}{\phi_\mathrm{m} - \phi}\right] + c_0(1-\phi)\left[\rho_{s,1}X + \rho_{s,2}(1-X)\right], \tag{4.9}$$

where $X \equiv \phi_1/\phi$, while $c_0 \equiv 2\cot\alpha/(9K_c)$ and $c_1 \equiv 2(K_v - K_c)/K_c$ are constants. As expected, Eq. (4.9) exactly matches the monodisperse model of [15, 16], when $X$ is set to 0 (i.e. $\phi_1 = 0$) or 1 (i.e. $\phi_2 = 0$). For equilibrium inside the thin film, we also require zero net flux of each particle species in the $z$-direction, $J_{z,i} = 0$, and set $J_{z,1}\phi_2 - J_{z,2}\phi_1 = 0$, which leads to

$$X' = c_2\frac{X(1-X)}{\sigma D_\mathrm{tr}}\left(\frac{\phi_\mathrm{m}}{\phi_\mathrm{m} - \phi}\right), \tag{4.10}$$

where $c_2 = 2(\rho_{s,2} - \rho_{s,1})\cot\alpha/9$.

The Eqs. (4.8)–(4.10) form a system of ODEs for the unknowns: $\phi$, $X$ and $\sigma$. Following [16], we define the scaled height $s = z/h$, where $h$ is the dimensionless film thickness, so that $\widetilde{\phi}(s) = \phi(hs)$, $\widetilde{X}(s) = X(hs)$, and $\widetilde{\sigma}(s) = \sigma(hs)/h$; tildes are subsequently dropped from the text. In addition, the average particle concentration $\phi_0$ and proportion of lighter particles $X_0$ correspond to:

$$\phi_0 = \int_0^1 \phi(s)\mathrm{d}s, \qquad X_0 = \frac{1}{\phi_0}\int_0^1 X(s)\phi(s)\mathrm{d}s. \tag{4.11}$$

For given $\phi_0$ and $X_0$ with $0 \le \phi_0 < \phi_\mathrm{m}$, the system has a unique solution for $s \in [0, 1]$. Solutions in Sect. 4.3 are computed via shooting in MATLAB, with an inclination angle fixed at $\alpha = 30°$ unless otherwise noted.

## 4.3 Results

We begin by briefly reviewing the monodisperse theory described by [15]. For the monodisperse system which consists of (4.9) and (4.8) with $X = 0$ or 1, there is a critical particle concentration $\phi_c$ such that $\phi(s)$ is monotone increasing (i.e. $\phi' > 0$) when $\phi_0 > \phi_c$ and monotone decreasing (i.e. $\phi' < 0$) when $\phi_0 < \phi_c$. The constant solution $\phi = \phi_c$ separating the two regimes is an unstable equilibrium. This bifurcation is illustrated in Fig. 4.2. In [15], the two regimes are referred to as 'ridged' and 'settled', respectively. Physically, ridged solutions describe aggregation of particles at the fluid surface, while a settled solution describes particles settling to the substrate, which leaves a clear fluid layer above. As there are two particle species to consider here, we denote as $\phi_{c,i}$ the critical concentration for the $i$th species in the

corresponding monodisperse problem ($X = 1$ for $i = 1$ and $X = 0$ for $i = 2$) and note that $\phi_{c,1} < \phi_{c,2}$ since the second particle is heavier. For $\alpha = 30°$, these values are $\phi_{c,1} = 0.459$ and $\phi_{c,2} = 0.521$ based on [15].

For the bidisperse system, we begin by discussing the structure of $X(s)$ and the mixing behaviour between particle species. As $s$ increases from 0 to 1, $X(s)$ consists of an interval with $X \approx 0$, followed by a transition region centred at $s = s_{\text{tr}}$, such that $X(s_{\text{tr}}) = 1/2$, and finally an interval with $X \approx 1$. The ODE (4.10) can be approximated near $s_{\text{tr}}$ as

$$X' \approx C^{-1} X(1 - X), \tag{4.12}$$

which has an explicit solution, $X(s) = 1 - \left(1 + \exp\left(\frac{s_{\text{tr}} - s}{C}\right)\right)^{-1}$. Here $C$ is the constant given by evaluating all other variables at $s = s_{\text{tr}}$:

$$C = \frac{9 \tan\alpha}{2(\rho_{s,2} - \rho_{s,1})} D_{\text{tr}}(\phi(s_{\text{tr}}))\sigma(s_{\text{tr}}) \left(1 - \frac{\phi(s_{\text{tr}})}{\phi_{\text{m}}}\right).$$

In order to quantify the amount of mixing between two particle species, we define the width of the mixing layer, $w$, to be the interval for which $0.05 < X < 0.95$. Based on the solution to (4.12), we find that $w \approx 5.9C$, valid for $w \ll 1$. Since the value of $C$ primarily depends on $\tan\alpha$, it can be shown that the mixing layer width, $w$, scales with $\tan\alpha$ (Fig. 4.3, right), and is approximately linear where the solution profiles are insensitive to changes in angle. This suggests that there will be little mixing for small inclination angles. Experimentally, [10] observed the bidensity slurry at low inclination angles to stratify into three layers of heavy particles, light particles, and clear fluid. This results in three distinct fronts flowing down the plane (Fig. 4.1, bottom right). At higher inclination angles they observed a 'ridged' regime with more mixing of particles, consistent with our theoretical predictions (Fig. 4.1, top right).

In order to investigate the bifurcation behaviour of bidensity slurries, we now consider the total concentration $\phi(s)$ and the individual concentrations, $\phi_1(s)$ and $\phi_2(s)$. Analogous to the monodisperse system, we call a solution 'settled' if neither species of particles are present up to the surface (i.e. $\phi = 0$ for some $s \in [0, 1]$), and 'ridged' if particles (of either kind) aggregate at the surface ($\phi \to \phi_{\text{m}}$ as $s \to 1$). Like the monodisperse case, the settled regime ($S$) corresponds to the case where $\phi$ is monotone decreasing. Monotonicity of solutions is important for analysis of the dynamic problem, which motivates a careful description of the equilibrium profiles in [26]. For the bidisperse system, $\phi$ is not necessarily monotonic in the ridged regime, but the individual concentrations $\phi_1$ and $\phi_2$ undergo similar transitions from decreasing to increasing as in the monodisperse case. Within the ridged regime, there exist critical concentrations $\phi_A$, $\phi_B$ and $\phi_C$ as functions of $X_0$, such that the profiles for $\phi$, $\phi_1$, and $\phi_2$ change from decreasing to mixed signs to increasing. This further partitions the ridged regime into three distinct sub-regions ($R_A$, $R_B$, and $R_C$), as summarized in Fig. 4.4. We now discuss each region in greater detail.

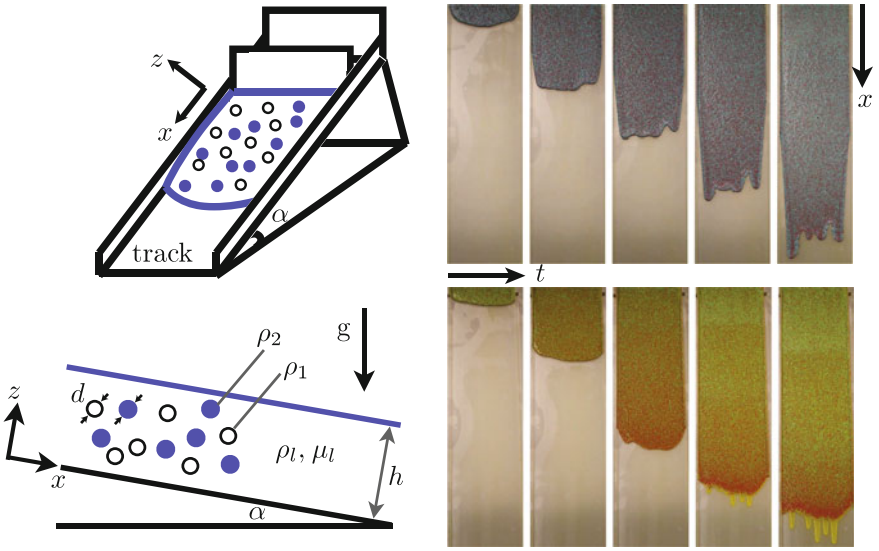


**Fig. 4.1** (*top left*) Schematic of the experimental apparatus; (*bottom left*) The thin film of fluid of $\rho_l$ and $\mu_l$ that contains two particle species of equal diameter $d$ and variant densities, such that $\rho_2 > \rho_1 > \rho_l$. Two sets of experimental results are shown on the right. In the *bottom right panel*, as time evolves (images from *left* to *right*), clear fingers form on the flow front, indicating that both particle species have settled to the channel walls with a clear fluid layer on top that moves ahead. On the other hand, the particles appear to remain aggregated and well-mixed on the front in the 'ridged' regime, as shown in the *top right panel*

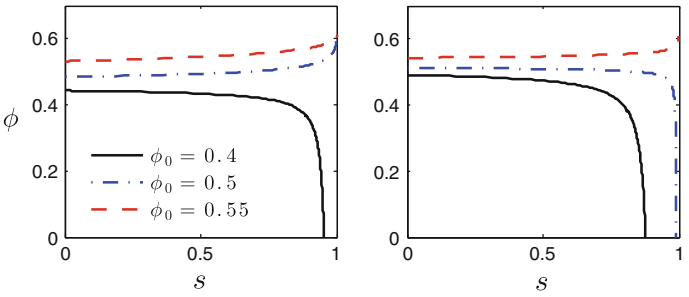


**Fig. 4.2** Transition from settled to ridged solutions in $\phi$ for the monodisperse system, for $X = 1$ (*left*) and $X = 0$ (*right*). The critical concentrations are $\phi_{c,1} = 0.459$ and $\phi_{c,2} = 0.521$

**Settled** ($0 < \phi_0 < \phi_A$): In the settled regime, the heavy particles settle to the substrate, with a layer of the lighter particles above, and then a clear fluid layer up to the free surface. The upper bound for the settled region, $\phi_A$ decreases from $\phi_{c,2}$ to $\phi_{c,1}$ as $X_0$ increases from 0 to 1. If $\phi_0 < \phi_{c,1}$, then the ODE system guarantees that $\phi$ is monotonically decreasing regardless of $X_0$.

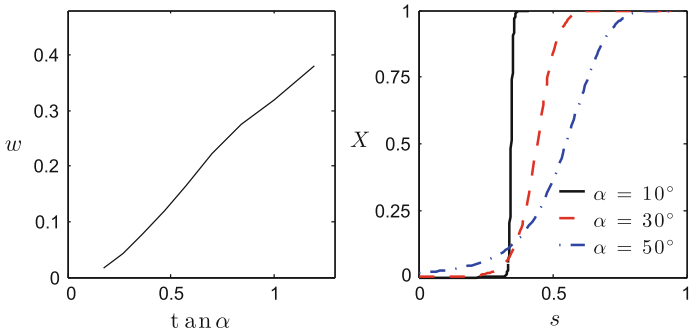


**Fig. 4.3** Dependence of the width $w$ of the mixing region (where $0.05 < X < 0.95$) on $\tan\alpha$; the relationship, shown on the *left*, is approximately linear. The *right panel* shows the $X$ profiles for $\alpha = 10, 30, 50°$

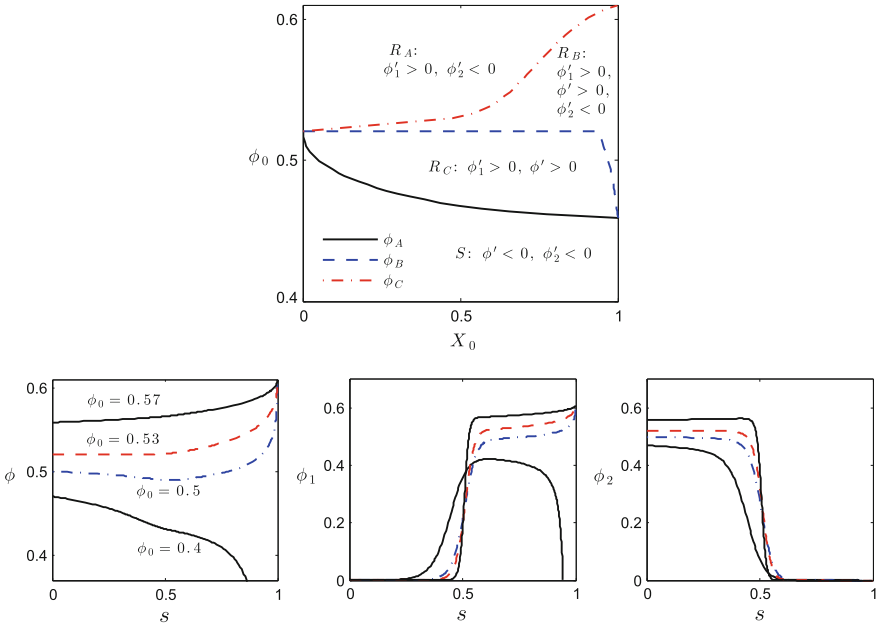


**Fig. 4.4** The *left panel* shows a phase diagram of solution regimes determined by total and relative concentrations $(X_0, \phi_0)$, separated by transition curves $\phi_A$, $\phi_B$ and $\phi_C$. Profiles in each region are shown below, for total concentration $\phi$ (*left*) and for the individual concentrations $\phi_1$, $\phi_2$

**Ridged A** ($\phi_A < \phi_0 < \phi_B$): When $\phi_{c,1} < \phi_0 < \phi_{c,2}$, the monodisperse theory suggests that the lighter species $\phi_1$ is more likely to aggregate on the free surface ($\phi_1 \to \phi_m$ as $s \to 1$) due to shear-induced migration while $\phi_2$ favours settling. Therefore, in this regime, $\phi_1$ is monotonically increasing (i.e. $\phi_1' > 0$) with the lighter particles mostly confined to a top region $[s_{tr}, 1]$. The heavier particles settle

so that $\phi_2' < 0$, with negligible but non-zero concentration beyond $s_{\text{tr}}$. Focusing on the top layer $[s_{\text{tr}}, 1]$ where $X \approx 1$, we view this as a perturbed version of the monodisperse bifurcation. As $\phi_0$ is increased across $\phi_A$, the average concentration of lighter particles in $[s_{\text{tr}}, 1]$ becomes large enough to produce a ridged solution.

**Ridged B** ($\phi_B < \phi_0 < \phi_C$): If $\phi_0 > \phi_{c,2}$, then $\phi$ is always monotone increasing ($\phi' < 0$), which defines this second ridged regime, $R_B$. The heavier particles still settle to the substrate as in the $R_A$ case, so that $\phi_2' < 0$. Note that, in the absence of tracer diffusivity (no mixing layer), $\phi_B = \phi_{c,2}$, unless $X = 1$ exactly, leading to $\phi_B = \phi_{c,1}$. This (discontinuous) $\phi_B$ closely approximates the actual curve in Fig. 4.4, which curves due to the mixing of particle layers but retains the same endpoints. There are two situations for $\phi_0 < \phi_{c,2}$ in which tracer diffusion can produce a ridged solution. First, if $\phi_0$ is very close to $\phi_{c,2}$, then even a small concentration of lighter particles can perturb the otherwise settled solution in the heavier layer so that $\phi' > 0$. Second, if $X_0$ is close to 1 and $\phi_0 > \phi_{c,1}$, then there is no well-defined settled layer of heavier particles, so the ridged behaviour of the lighter layer ensures that $\phi' > 0$.

**Ridged C** ($\phi_C < \phi_0 < \phi_{\text{m}}$): For sufficiently large $\phi_0$, the average concentration of $\phi_2$ near $s = 0$ (where $X \approx 0$) is large enough to produce an initially increasing solution in $\phi_2$. Thus, distinct from $R_A$ and $R_B$, the heavier particles tend to migrate away from the substrate in this last ridged regime. However, the lighter particles displace the heavier particles near the free surface so that $\phi_2 \to 0$. Hence $\phi_2$ is still not monotone increasing—it eventually decreases sharply to nearly zero around $s_{\text{tr}}$.

## 4.4 Conclusions

The same pattern of transitions is also observed for fixed $\phi_0$ with varying $X_0$ and $\alpha$, both experimentally and theoretically. As with increasing $\phi_0$, an increase in $\alpha$ has the effect of altering the balance of fluxes to favour shear-induced migration, in this case by reducing the normal component of gravity [15]. The previous discussion applies to the $(X_0, \alpha)$ plane as well, and, in particular, there is a critical $\alpha_A(X_0)$, analogous to $\phi_A(X_0)$, separating settled and ridged solutions. The predicted bifurcation is shown in Fig. 4.5 along with experimental results [10] identifying settled or ridged behaviour. Experiments to date have not measured the particle concentrations inside the thin film and thus do not distinguish between different theoretically predicted types of ridged behaviour. Overall, the current theory captures the bifurcation curve obtained experimentally, although the critical angles predicted by the model are greater than what is measured in the experiment by about five degrees. This discrepancy can be attributed primarily to the value of the empirical parameter $K_c$. While we based the value of $K_c$ on [15, 16], the types of beads used in [10] differ slightly in size and texture from the previous experiments and warrant further experiments to better estimate $K_c$.

In this chapter, we derive a diffusive model of bidensity suspensions flowing down an incline and use it to describe the normal equilibrium of the suspensions inside the thin film. The mixture consists of the viscous fluid of density, $\rho_l$, and two negatively

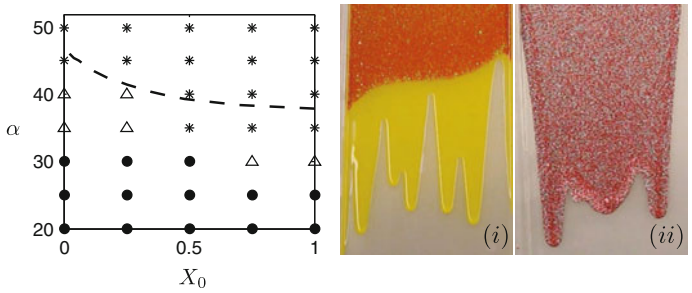


**Fig. 4.5** (*Left*) Bifurcation $\alpha_A(X_0)$ (*dashed line*) between settled and ridged regimes for fixed $\phi_0 = 0.4$ with varying $\alpha$ and $X_0$. The symbols indicate experimental results identified as ridged (*star*) or settled (*circle*). The *triangles* mark results for which the particles did not equilibrate in the duration of the experiment. (*Right*) Photographs of the experiment in the settled and ridged regimes are shown on the *right* for experimental parameters, (i) $\alpha = 20°$, $X_0 = 0.5$ and (ii) $\alpha = 50°$, $X_0 = 0.5$

buoyant particle species of the equal diameter, $d$, and variant densities, such that $\rho_2 > \rho_1 > \rho_l$. In the monodisperse case of the same geometry, heavy particles in the viscous fluid were shown to either settle rapidly to the channel walls ('settled' regime) or collect on the free surface ('ridged'), depending on the channel inclination angle and the total volume fraction. This bifurcation behaviour was explained by [2, 15, 16] by balancing particle fluxes due to sedimentation and drift diffusion. The analogous bifurcation behaviour was observed in bidensity suspensions experimentally by [10] and is explained by our current equilibrium model.

Notably, additional complexities arise due to the presence of a second particle species. For instance, the ridged regime in the bidensity suspensions now consists of three sub-regimes ($R_A$, $R_B$, and $R_C$) that display different profiles of $\phi_1$ and $\phi_2$, depending on the relative particle volume fraction, $X_0$. It would be interesting to explore the sub-regimes in future experiments, which would require new experimental techniques to measure the volume concentration of different particle species through the layer. In addition, the mixing behaviour between particle species is investigated by incorporating tracer diffusion in our model. This mixing effect is shown to depend on the inclination angle, such that lower angles lead to less mixing. This behaviour has been observed experimentally in [10] where they found the bidensity mixture to stratify into separate layers forming three distinct fronts at smaller inclination angles. Therefore, our equilibrium model and experimental observations suggest that particle segregation is more pronounced in the 'settled' regime, while particles remain well-mixed in the 'ridged' regime.

Particle segregation is fundamentally important in oil refinement, waste-water treatment, and mineral processing via a spiral separator. However, these applications lack quantitative models that are important for predictive design. Recently, [8, 9] demonstrated that the equilibrium model for monodisperse slurries on an incline is valid in spiral geometries to leading order and derived a simple steady state model. We believe the present model could lead to a valid equilibrium theory for more

general polydisperse slurry segregation models in helical domains. Furthermore, such equilibrium models are the building blocks for the development of implicit flux functions for dynamic transport models [14, 16, 26]. The current bidensity theory may lead to new dynamic models that could predict multilayer stratified flows as observed in [10].

**Acknowledgments** This work is supported by NSF grants DMS-1312543 and DMS-1048840 and UC Lab Fees Research Grant 09-LR-04-116741-BERA.

## References

1. Breedveld, V., van den Ende, D., Tripathi, A., Acrivos, A.: The measurement of the shear-induced particle and fluid tracer diffusivities in concentrated suspensions by a novel method. J. Fluid Mech. **375**, 297–318 (1998)
2. Cook, B.P.: Theory for particle settling and shear-induced migration in thin-film liquid flow. Phys. Rev. E **78**, 045303 (2008)
3. Couturier, É., Boyer, F., Pouliquen, O., Guazzelli, É.: Suspensions in a tilted trough: second normal stress difference. J. Fluid Mech. **686**, 26–39 (2011)
4. Davis, R.H., Acrivos, A.: Sedimentation of noncolloidal particles at low Reynolds numbers. Annu. Rev. Fluid Mech. **17**, 91 (1985)
5. Eckstein, E.C., Bailey, D., Shapiro, A.H.: Self-diffusion of particles in shear flow of a suspension. J. Fluid Mech. **79**, 191–208 (1977)
6. Gadala-Maria, F., Acrivos, A.: Shear induced structure in a concentrated suspension of solid spheres. J. Rheol. **24**(6), 799–814 (1980)
7. Krishnan, G.P., Beimfohr, S., Leighton, D.T.: Shear-induced radial segregation in bidisperse suspensions. J. Fluid Mech. **321**, 371–393 (1996)
8. Lee, S., Stokes, Y.M., Bertozzi, A.L.: A model for particle laden flow in a spiral concentrator. In: 23rd International Congress of Theoretical and Applied Mechanics (ICTAM) Procedia IUTAM (2012)
9. Lee, S., Stokes, Y.M., Bertozzi, A.L.: Behavior of a particle-laden flow in a spiral channel. Phys. Fluids **26**, 043302 (2014)
10. Lee, S., Mavromoustaki, A., Urdaneta, G., Huang, K., Bertozzi, A.L.: Experimental investigation of bidensity slurries on an incline. Granul. Matter **16**(2), 269–274 (2014)
11. Leighton, D., Acrivos, A.: Viscous resuspension. Chem. Eng. Sci. **41**, 1377–1384 (1986)
12. Leighton, D., Acrivos, A.: Shear-induced migration of particles in concentrated suspensions. J. Fluid Mech. **181**, 415 (1987)
13. Leighton, D., Acrivos, A.: Measurement of shear-induced self-diffusion in concentrated suspensions of spheres. J. Fluid Mech. **177**, 109–131 (1987)
14. Mavromoustaki, A., Bertozzi, A.L.: Hyperbolic systems of conservation laws in gravity-driven, particle-laden thin-film flows. J. Eng. Math. **88**, 29–48 (2014)
15. Murisic, N., Ho, J., Hu, V., Latterman, P., Koch, T., Lin, K., Mata, M., Bertozzi, A.L.: Particle-laden viscous thin-film flows on an incline: experiments compared with an equilibrium theory based on shear-induced migration and particle settling. Physica D **240**, 1661–1673 (2011)
16. Murisic, N., Pausader, B., Peschka, D., Bertozzi, A.L.: Dynamics of particle settling and resuspension in viscous liquid films. J. Fluid Mech. **717**, 203–231 (2013)
17. Nott, P.R., Brady, J.F.: Pressure-driven flow of suspensions: simulation and theory. J. Fluid Mech. **275**, 157–199 (1994)
18. Oron, A., Davis, S.H., Bankoff, S.G.: Long-scale evolution of thin liquid films. Rev. Mod. Phys. **69**, 931 (1997)

19. Phillips, R.J., Armstrong, R.C., Brown, R.A., Graham, A.L., Abbott, J.R.: A constitutive equation for concentrated suspensions that accounts for shear-induced particle migration. Phys. Fluids **4**, 30–40 (1992)
20. Ramachandran, A., Leighton, D.T.: Viscous resuspension in a tube: the impact of secondary flows resulting from second normal stress differences. Phys. Fluids **19**(5), 053301 (2007)
21. Ramachandran, A., Leighton, D.T.: The effect of gravity on the meniscus accumulation phenomenon in a tube. J. Rheol. **51**, 1073–1098 (2007)
22. Revay, J.M., Higdon, J.J.L.: Numerical simulation of polydisperse sedimentation: equal-sized spheres. J. Fluid Mech. **243**, 15–32 (1992)
23. Sierou, A., Brady, J.F.: Shear-induced self-diffusion in non-colloidal suspensions. J. Fluid Mech. **506**, 285–314 (2004)
24. Timberlake, B.D., Morris, J.F.: Particle migration and free-surface topography in inclined plane flow of a suspension. J. Fluid Mech. **538**, 309–341 (2005)
25. Tripathi, A., Acrivos, A.: Viscous resuspension in a bidensity suspension. Int. J. Multiph. Flow **25**(1), 1–14 (1999)
26. Wang, L., Bertozzi, A.L.: Shock solutions for high concentration particle-laden thin films. SIAM J. Appl. Math. **74**, 322–344 (2014)